Microwave conductance of aligned multiwall carbon nanotube textile sheets

Brian L. Brown,[1] Julia S. Bykova,[1,2] Austin R. Howard,[1,2] Anvar A. Zakhidov,[1,2] Eric A. Shaner,[3] and Mark Lee[1]
[1]*Department of Physics, The University of Texas at Dallas, Richardson, Texas 75080, USA*
[2]*The Alan G. McDiarmid NanoTech Institute, The University of Texas at Dallas, Richardson, Texas 75080, USA*
[3]*Sandia National Laboratories, Albuquerque, New Mexico 87123, USA*

(Received 22 August 2014; accepted 17 December 2014; published online 30 December 2014)

Multiwall carbon nanotube (MWNT) sheets are a class of nanomaterial-based multifunctional textile with potentially useful microwave properties. To understand better the microwave electrodynamics, complex AC conductance measurements from 0.01 to 50 GHz were made on sheets of highly aligned MWNTs with the alignment texture both parallel and perpendicular to the microwave electric field polarization. In both orientations, the AC conductance is modeled to first order by a parallel frequency-independent conductance and capacitance with no inductive contribution. This is consistent with low-frequency diffusive Drude AC conduction up to 50 GHz, in contrast to the "universal disorder" AC conduction reported in many types of single-wall nanotube materials.
 [http://dx.doi.org/10.1063/1.4905220]

While carbon nanotubes (CNTs) are fascinating nanomaterials in and of themselves, the ability to assemble CNTs into macroscopic yarns[1–3] and sheets[4,5] has resulted in nanomaterial-based multifunctional textiles with widely useful mechanical,[4,6] thermal,[7] optical,[4,8] and electrical[4,5] properties. Sheets composed of long, highly aligned multiwall nanotubes (MWNTs) can have a DC resistance anisotropy ratio of 10 to 100 between current flow perpendicular and parallel to the prevailing MWNT alignment.[4] This electrical anisotropy and the fact that a sheet is composed of MWNTs 10 to 20 nm in diameter, usually grouped into strands ~100 nm thick spaced 0.1 to 0.5 μm apart, mean that MWNT sheets can be used as wire grid polarizers for infrared light.[4] Other demonstrated applications for CNT based textiles include thermoacoustic loudspeakers,[9] supercapacitors,[10] and high-power microwave absorbers.[11,12]

Although many mechanical and DC electrical properties of CNT-based textiles have been reported, much less attention has been paid to their microwave properties. Relatively little is known about the physical mechanisms governing or even the values of basic linear AC properties such as microwave conductance. Understanding AC response is critical to all high-frequency and high-speed electronic applications of these materials. Microwave conductance has been measured on many types of single wall nanotube (SWNT) materials in the form of self-assembled arrays,[13,14] thin-film networks,[15,16] and semiconducting and metallic SWNT "paper"[17] and "mats."[18] Interestingly, the microwave conductance of SWNTs in the tens of GHz range in most,[13–17] but not all[18] these formats, has been described by a "universal disorder" or glass-like electrodynamic response.[19] Whether a similar AC conduction mechanism holds for MWNT textiles has not been known until now.

In this letter, we directly address these gaps in knowledge by reporting measurements and modeling of the complex microwave conductance of highly aligned MWNT textile sheets across a broad frequency range of 0.01 to 50 GHz with the MWNT strands orientated parallel and perpendicular to the microwave field polarization. The major features of the MWNT sheet conductance vs. frequency can be approximately modeled by a frequency-independent resistor and capacitor consistent with conventional low-frequency diffusive AC conduction,[20] in contrast to glassy universal-disorder dynamics seen in many SWNT materials.

A MWNT forest was grown by catalytic chemical vapor deposition (CVD) on a silicon substrate seeded with a 3 nm iron catalyst film deposited by electron-beam evaporation. For MWNT growth, a He/H_2 (30%)/C_2H_2 (2%) gas mixture was flowed at 1020 sccm through a quartz tube CVD reactor at 700 °C and 1 atm pressure for 10 min. The MWNTs in the forest averaged 420 μm high with an areal mass density of 3.4 μg/cm^2. A self-supporting highly aligned MWNT sheet 8 mm wide, several cm long, with areal density of 2.7 μg/cm^2 was dry-drawn from the sidewall of this forest in the manner described in detail in Ref. 4. Segments ~1 cm long by 0.5 cm wide were cut from this sheet and assembled over the ground-signal-ground (*g-s-g*) gaps of co-planar waveguides (CPWs) designed for broadband microwave measurements (Fig. 1(a)). Each MWNT sheet was adhered to its CPW by wetting with drops of isopropanol and subsequent alcohol evaporation. The surface tension during evaporation densified the MWNT sheet, reducing its thickness from 20 to 50 μm down to ~0.2 μm. Scanning electron microscope inspection (Fig. 1(b)) showed that the densified MWNT sheets were composed of long, highly aligned MWNT strands interconnected by thinner bundles of tubes to create a laterally extended network with a dominant directional alignment. Two-point DC resistance measurements using silver print contacts gave sheet resistances (including contact resistance) of 7100 ± 1120 Ω/□ for current perpendicular (⊥) to the strand alignment and 540 ± 46 Ω/□ for current parallel (∥) to the alignment for an anisotropy ratio $R(\perp)/R(\parallel)$ =

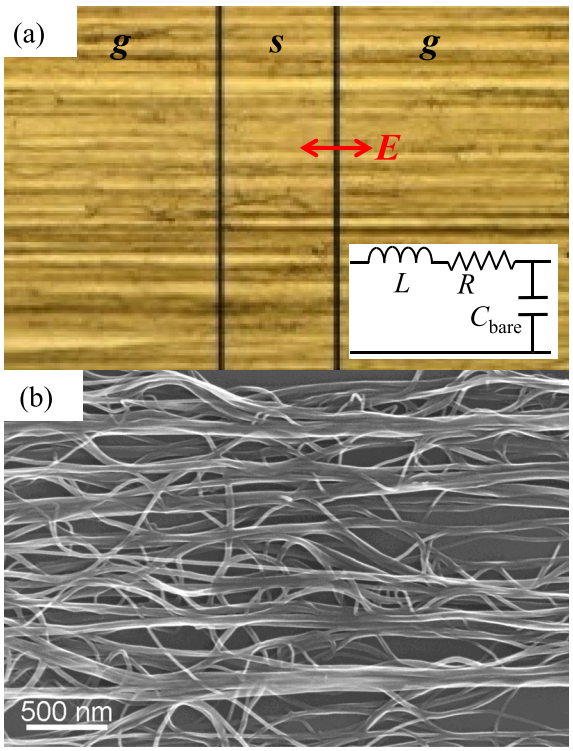

FIG. 1. (a) Optical microscope image of a MWNT sheet assembled over the Au ground-signal-ground (*g*-*s*-*g*) conductors of a CPW, with the MWNT strands aligned parallel to the electric field (***E***) polarization across the gaps (indicated by the red arrow). The *g*-*s*-*g* gaps are both 3 μm wide. Inset: Transmission line model of a bare CPW. *L* and *R* are the series inductance and resistance and C_{bare} is the bare shunt capacitance (all per unit length). (b) Scanning electron microscope image of a segment of the MWNT sheet showing bundles, fibrils, and forks.

13 ± 3.3. The electrical properties of the densified sheets were stable over several weeks to months in ordinary room conditions, although they were highly susceptible to mechanical damage (e.g., fraying or peeling) if improperly handled.

Construction and characterization of the CPWs are described in detail in Ref. 13. All CPWs were 1.0 cm long Au-on-fused quartz with 3 μm gaps between the signal and the two ground conductors and were designed for 50 Ω characteristic impedance. The CPWs had 100 nm of Si_3N_4 insulating the Au *g*-*s*-*g* conductors so that the MWNT sheets coupled capacitively to the microwave field. In this way, contact resistance effects were avoided, while the contact capacitance can be extracted from analysis of low frequency dependence. Two sheet alignments were examined: dominant MWNT strand orientation aligned (1) parallel (∥) and (2) perpendicular (⊥) to the polarization of the microwave electric field in the CPW gaps (Fig. 1(a), inset of Fig. 2(b), and inset of Fig. 3(b)). For each orientation, three separate samples were measured. Among samples of same orientation, all qualitative frequency dependencies were reproducible, and quantitative agreement in measured values was within 10%.

Phase-sensitive microwave reflection and transmission measurements were made using a two-port vector network analyzer (VNA) (Agilent N5245A). VNA signals were coupled to/from a CPW using a pair of 150 μm pitch *g*-*s*-*g* probes (GGB 67A-GSG-150) touched down at either end of the CPW. The system was calibrated across the 0.01–50

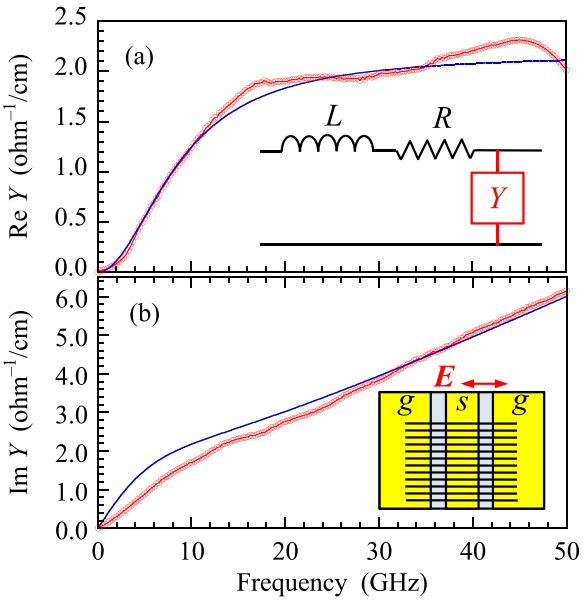

FIG. 2. Shunt conductance *Y* per unit length for a CPW with MWNT sheet aligned parallel to the microwave polarization. (a) Real *Y* from data (red circles) and computed from a circuit model (blue solid curve). Inset: transmission line model with generalized *Y* due to the MWNT sheet. (b) Imaginary *Y* from data (red circles) and computed from a circuit model (blue solid curve). Inset: Illustration of a MWNT sheet assembled on a CPW with strands oriented parallel to the electric field (***E***) polarization near the gaps.

GHz band to 50 Ω impedance up to the plane of the probe tips using a commercial short-open-load-thru calibration substrate (GGB CS-5). All data presented were taken at ambient room temperature with samples in vacuum to prevent air or moisture adsorption. Magnitudes and phases of the voltage scattering or *S*-parameters S_{ij} ($i,j = 1, 2$) were recorded as a function of frequency, *f*. The CPWs, with and without

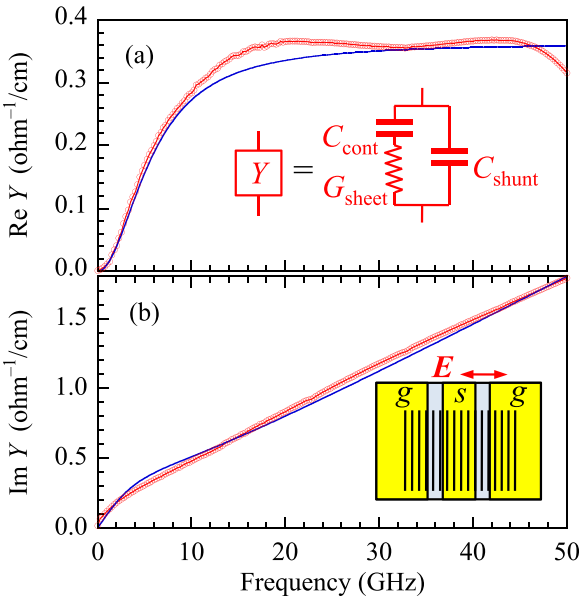

FIG. 3. Shunt conductance *Y* per unit length for a CPW with MWNT sheet aligned perpendicular to the microwave polarization. (a) Real *Y* from data (red circles) and computed from a circuit model (blue solid curve). Inset: circuit model for the generalized *Y* depicted in the inset of Fig. 2(a). (b) Imaginary *Y* from data (red circles) and computed from a circuit model (blue solid curve). Inset: Illustration of a MWNT sheet assembled on a CPW with strands oriented perpendicular to the electric field (***E***) polarization near the gaps.

MWNT sheet, were symmetric with respect to the waveguide ports (indexed 1 and 2) at either end of the CPWs, so the reflection parameter (return loss) $S_{11} = S_{22}$ and transmission parameter (insertion loss) $S_{21} = S_{12}$ to within experimental accuracy. Experimental procedure was as follows: *S*-parameters were first measured for "bare" CPWs, i.e., CPWs with no MWNT sheet. The *S*-parameters of all bare CPWs were the same to within 5% variance. MWNT sheets were then assembled on designated CPWs and the *S*-parameters of these "assembled" CPWs, i.e., CPWs with MWNT sheet, were re-measured. One CPW was left bare as a control to monitor systematic repeatability of measurements taken prior to and after MWNT sheet assembly. Post-assembly measurements showed that the control CPW's *S*-parameters matched the bare CPWs' to within the original 5% variance.

All bare CPWs had $|S_{11}|$ between –20 and –25 dB across most of the measurement band, indicating a reasonable impedance match to the 50 Ω system, and $|S_{21}|$ between –2 and –11 dB. The bare $|S_{21}|$'s frequency dependence was well modeled by the series surface resistance loss of the Au electrodes. Assembling MWNT sheets on the CPWs caused $|S_{11}|$ to increase to –3.5 to –6 dB in ∥ and –5 to –8 dB in ⊥ orientation, showing that the MWNT sheet caused significant impedance mismatch. $|S_{21}|$ of the assembled CPWs in both parallel and perpendicular orientations fell to between –13 and –59 dB across the measurement band, indicating that the MWNT sheet also introduced significant shunt loss.

Because fused quartz and silicon nitride have low loss tangents ($\sim 10^{-4}$) and Au is highly conductive, the bare/control CPWs were accurately modeled as standard lossy transmission lines[21] with series (signal in to signal out) inductance *L* and resistance *R* per unit length of transmission line and shunt (signal to ground) conductance per unit length due solely to the capacitance between signal and ground conductors. The bare CPW transmission line schematic is illustrated in the inset of Fig. 1(a). A standard analysis[21] of the bare/control CPW *S*-parameters yields the bare shunt capacitance (per unit length of transmission line) $C_{\text{bare}} = 1.2 \pm 0.05$ pF/cm, including the Si_3N_4. The assembly of a MWNT sheet across the *g-s-g* gaps adds an additional AC shunt path to the transmission line with a shunt conductance *Y* that may not be simply capacitive. The *Y* arising from the MWNT sheet changes the propagation constant and impedance of the CPW and so changes the *S*-parameters.

The shunt conductance *Y* of each assembled CPW was determined from the *S*-parameters using the standard transmission line de-embedding procedure detailed in Ref. 22. The inset of Fig. 2(a) illustrates the transmission line schematic used for an assembled CPW with *Y* (not assumed to be purely capacitive) instead of the C_{bare} of the bare CPW. The resulting real and imaginary *Y* are shown in Fig. 2 for ∥ and Fig. 3 for ⊥ orientation using red circle markers. In both orientations, Re *Y* shows a low-frequency roll-off and becomes only weakly frequency dependent at high frequencies. Also in both orientations, the high-frequency Im *Y* is to first order a linear function of frequency.

The general features of *Y*(*f*) shown in Figs. 2 and 3 suggest a simple circuit model that can at least describe the main characteristics in both ∥ and ⊥ orientations. The low-frequency roll-off in Re *Y* is directly attributable to the capacitive contact between MWNT sheet and Au electrodes. This is simply modeled with a contact capacitance C_{contact} blocking low-frequency in-phase AC shunt current through the MWNT sheet. The observation that at high frequencies Re *Y* is only weakly frequency dependent suggests that the in-phase shunt conductance of the MWNT sheet itself can be approximately modeled by a shunt resistor with frequency-independent conductance (per unit length of transmission line) G_{sheet} in series with C_{contact}. The linear behavior of Im *Y* at high frequency indicates that the displacement current gives a reactive shunt conductance that can be modeled by a frequency independent parallel capacitance C_{shunt}. Physically, C_{shunt} results from the polarizability of the MWNT sheet filling in the near-surface *g-s-g* gap volumes that were occupied by vacuum in the bare CPW. Thus, assembly of the MWNT sheet introduces a relative permittivity $\varepsilon_r > 1$ in the gaps and causes $C_{\text{shunt}} > C_{\text{bare}}$.

The resulting simple circuit model for *Y*(*f*) is schematically illustrated in the inset of Fig. 3(a). From this circuit model, Re *Y* and Im *Y* in both ∥ and ⊥ orientations were calculated and are plotted as solid blue curves in Figs. 2 and 3. For ∥ (Fig. 2), circuit parameters used for both Re *Y* and Im *Y* are: $G_{\text{sheet}} = 2.2\ \Omega^{-1}$/cm, $C_{\text{shunt}} = 18$ pF/cm, and $C_{\text{contact}} = 40$ pF/cm. For ⊥ (Fig. 3), circuit parameters used for both Re *Y* and Im *Y* are: $G_{\text{sheet}} = 0.35\ \Omega^{-1}$/cm, $C_{\text{shunt}} = 5.6$ pF/cm, and $C_{\text{contact}} = 10$ pF/cm. These are not optimized fitting parameters since one set of values is used to describe both Re *Y* and Im *Y*—they should be taken as coarse values that capture the major frequency trends of the complex conductances. Also, it is clear that the *Y*(*f*) data show finer frequency dependent details that cannot be described by any reasonably simple circuit model.

The circuit model values given above are physically reasonable. Following Ref. 14, estimating the contact capacitance between Au ground plane and an array of oriented MWNTs, using the sizes and densities in this MWNT sheet, separated by 100 nm of Si_3N_4 gives a contact capacitance of order 10 to 100 pF/cm. On samples where MWNT sheet samples were assembled in ∥ orientation on CPWs without Si_3N_4, 2-point DC resistance measurements gave DC shunt conductance of $G_{\text{DC}} = 1$ to $2\ \Omega^{-1}$/cm. This is somewhat less that the $2.2\ \Omega^{-1}$/cm drawn from the *Y*(*f*) circuit model, but the difference is within the range of possible contact resistance. The sheet conductance anisotropy ratio is then $G_{\text{sheet}}(\|)/G_{\text{sheet}}(\perp) = 6.3$, about half of the 2-point DC resistance anisotropy ratio $R(\perp)/R(\|)$. Again, however, possible anisotropy in contact resistance is not accounted for in the DC measurements. Finally, the sole difference in shunt capacitance geometry between bare and assembled CPWs is the filling of vacuum by MWNT sheet in the volume near the *g-s-g* gaps. Thus, the ratio $C_{\text{shunt}}/C_{\text{bare}}$ should give a measure of ε_r of the MWNT sheet. The modeled data give $\varepsilon_r(\|) \approx C_{\text{shunt}}/C_{\text{bare}} = 15$ and $\varepsilon_r(\perp) \approx C_{\text{shunt}}/C_{\text{bare}} = 4.7$. Since on physical grounds the polarizability in ∥ orientation should be larger than that in ⊥ orientation, it is reasonable that the derived $\varepsilon_r(\|)/\varepsilon_r(\perp) > 1$.

It is of interest to compare these results to existing work on MWNT and SWNT materials in various formats. The MWNT sheet conductance reported here is generally consistent with low-frequency diffusive (Drude) AC conduction $\sigma(f)$,[20] where in the low frequency limit (excluding contacts)

Re $\sigma \approx$ constant and Im $\sigma \propto f$. In Drude conduction, when f exceeds the mean scattering rate, inertial effects appear as an inductance[23,24] causing Re σ and Im σ to roll off at high frequencies. The lack of inductive contribution in $Y(f)$ implies that the MWNT sheets' AC dynamics are dominated by diffusive scattering up to 50 GHz. This is consistent with prior reports of single MWNTs being diffusive conductors[25] even though in the textile format one expects significantly more scattering due to kinks and intersections between strands, particularly in $\perp$ orientation. A Drude-like mechanism is also consistent with AC results reported for SWNT "mats."[18] However, AC results on several other SWNT formats[13–17] report an AC conductance having a sub-linear frequency dependence $Y(f) \propto f^{s}$ for $0 < s < 1$ from ~1 to 50 GHz. This behavior is interpreted as "universal disorder" AC dynamics[19] from a random glass-like distribution of scattering potentials rather than ordinary diffusion. It is unclear what microscopic material conditions differentiate between glass-like and diffusive AC dynamics.

Further comparing our results to the literature, the values $\varepsilon_r(\|) \approx 15$ and $\varepsilon_r(\perp) \approx 5$ obtained for MWNT sheets are similar to the Re $\varepsilon_r = 5$ to 20 (from 20 to 50 GHz) reported in Ref. 26 for various densities of SWNT/MWNT mixtures with Ni and Y impurities. Moreover, our results show no evidence of very large microwave permittivity as reported for composites of MWNTs,[27] SWNTs,[28] and SWNT/MWNT mixtures at high densities and low frequencies.[26] The distinction may be that the MWNT sheets used here were 100% CNT material forming a self-supporting network without impurities or binders. It is possible that large permittivity effects are characteristic of impurity or binder interactions at high densities. Finally, our results also do not show evidence for highly efficient microwave absorption that has been reported for MWNT bundles, fibers, and mixtures at high power.[11,12,29] In these works, strong microwave heating was observed using typically several hundred watts of microwave power, compared to the microwatts used for the measurements presented here. Thus, the results reported here are fundamentally linear response properties, whereas the strong microwave absorption may be due to nonlinear effects only observable at high powers.[29]

In summary, we measured the real and imaginary AC conductance of CNT textile sheets composed of aligned MWNT strands oriented both parallel and perpendicular to the electric field polarization. Up to 50 GHz, the real conductance in both orientations can be approximately modeled to first order by a frequency independent conductance with a conductance anisotropy ratio $G_{\text{sheet}}(\|)/G_{\text{sheet}}(\perp) \approx 6$. The reactance in both orientations can be modeled by a frequency independent capacitance which yields a permittivity anisotropy ratio $\varepsilon_r(\|)/\varepsilon_r(\perp) \approx 3$. The AC transport through the CNT sheet is consistent with simple diffusive scattering up to 50 GHz, in direct contrast to the glassy AC conductance reported in many forms of SWNT material. These results provide useful physical input values and understanding for the quantitative modeling and design of many possible microwave applications of MWNT sheets, such as microwave-driven selective heating,[30] electromagnetic interference (EMI) shielding,[31] and microwave radiation induced electrochemistry.[32]

Work at Sandia and UTD Department of Physics was supported by the DOE Office of Basic Energy Sciences. Sandia National Laboratories is a multi-program laboratory managed and operated by Sandia Corporation, a wholly owned subsidiary of Lockheed Martin Corporation, for the U.S. Department of Energy's National Nuclear Security Administration under Contract No. DE-AC04-94AL85000. Work at the UTD McDiarmid NanoTech Institute was supported by the U.S. Air Force Office of Scientific Research (via Contract No. FA9550-09-1-0384 on "Strengthening Superconductivity in Nanostructures").

[1]K. Jiang, Q. Li, and S. Fan, Nature **419**, 801 (2002).
[2]M. Zhang, K. R. Atkinson, and R. H. Baughman, Science **306**, 1358 (2004).
[3]M. D. Lima, S. Fang, X. Lepró, C. Lewis, R. Ovalle-Robles, J. Carretero-González, E. Castillo-Martínez, M. E. Kozlov, J. Oh, N. Rawat, C. S. Haines, M. H. Haque, V. Aare, S. Stoughton, A. A. Zakhidov, and R. H. Baughman, Science **331**, 51 (2011).
[4]M. Zhang, S. Fang, A. A. Zakhidov, S. B. Lee, A. E. Aliev, C. D. Williams, K. R. Atkinson, and R. H. Baughman, Science **309**, 1215 (2005).
[5]K. Liu, Y. Sun, L. Chen, C. Feng, X. Feng, K. Jiang, Y. Zhao, and S. Fan, Nano Lett. **8**, 700 (2008).
[6]S. Fang, M. Zhang, A. A. Zakhidov, and R. H. Baughman, J. Phys.: Condens. Matter **22**, 334221 (2010).
[7]A. E. Aliev, C. Guthy, M. Zhang, S. Fang, A. A. Zakhidov, J. E. Fischer, and R. H. Baughman, Carbon **45**, 2880 (2007).
[8]X. M. Liu, H. R. Gutiérrez, and P. C. Eklund, J. Phys.: Condens. Matter **22**, 334213 (2010).
[9]L. Xiao, Z. Chen, C. Feng, L. Liu, Z.-Q. Bai, Y. Wang, L. Qian, Y. Zhang, Q. Li, K. Jiang, and S. Fan, Nano Lett. **8**, 4539 (2008).
[10]D. Yu and L. Dai, J. Phys. Chem. Lett. **1**, 467 (2010).
[11]K. R. Paton and A. H. Windle, Carbon **46**, 1935 (2008).
[12]E. Vázquez and M. Prato, ACS Nano **3**, 3819 (2009).
[13]C. Highstrete, E. A. Shaner, M. Lee, F. E. Jones, P. M. Dentinger, and A. A. Talin, Appl. Phys. Lett. **89**, 173105 (2006).
[14]C. Highstrete, M. Lee, A. A. Talin, and A. L. Vance, Appl. Phys. Lett. **95**, 203111 (2009).
[15]H. Xu, S. M. Anlage, L. Hu, and G. Grüner, Appl. Phys. Lett. **90**, 183119 (2007).
[16]H. Xu, S. Zhang, S. M. Anlage, L. Hu, and G. Grüner, Phys. Rev. B **77**, 075418 (2008).
[17]J. S. Bulmer, J. Martens, L. Kurzepa, T. Gizewski, M. Egilmez, M. G. Blamire, N. Yahya, and K. K. K. Koziol, Sci. Rep. **4**, 3762 (2014).
[18]O. Hilt, H. B. Brom, and M. Ahlskog, Phys. Rev. B **61**, R5129 (2000).
[19]J. C. Dyre and T. B. Schroder, Rev. Mod. Phys. **72**, 873 (2000).
[20]N. W. Ashcroft and N. D. Mermin, *Solid State Physics* (Saunders College, New York, 1976), Chap. 1.
[21]D. M. Pozar, *Microwave Engineering*, 4th ed. (John Wiley & Sons, Inc., Hoboken, NJ, 2012), Chap. 2.
[22]J. Zhang and T. Y. Hsiang, PIERS Online **3**, 1102 (2007).
[23]P. J. Burke, I. B. Spielman, J. P. Eisenstein, L. N. Pfeiffer, and K. W. West, Appl. Phys. Lett. **76**, 745 (2000).
[24]M. Lee, L. N. Pfeiffer, and K. W. West, Appl. Phys. Lett. **81**, 1243 (2002).
[25]A. Bachtold, M. S. Fuhrer, S. Plyasunov, M. Forero, E. H. Anderson, A. Zettl, and P. L. McEuen, Phys. Rev. Lett. **84**, 6082 (2000).
[26]E. Decrossas, M. A. El Sabbagh, V. F. Hanna, and S. M. El-Ghazaly, IEEE Trans. Electromagn. Compat. **54**, 81 (2012).
[27]J. Wu and L. Kong, Appl. Phys. Lett. **84**, 4956 (2004).
[28]S. H. Park, P. Thielemann, P. Asbeck, and P. R. Bandaru, Appl. Phys. Lett. **94**, 243111 (2009).
[29]Z. Ye, W. D. Deering, A. Krokhin, and J. A. Roberts, Phys. Rev. B **74**, 075425 (2006).
[30]A. L. Higginbotham, P. G. Moloney, M. C. Waid, J. G. Duque, C. Kittrell, H. K. Schmidt, J. J. Stephenson, S. Arepalli, L. L. Yowell, and J. M. Tour, Compos. Sci. Technol. **68**, 3087 (2008).
[31]B. Q. Yuan, L. M. Yu, L. M. Sheng, K. An, and X. L. Zhao, J. Phys. D: Appl. Phys. **45**, 235108 (2012).
[32]J. G. Duque, M. Pasquali, and H. K. Schmidt, J. Am. Chem. Soc. **130**, 15340 (2008).

2014-12

Microwave Conductance of Aligned Multiwall Carbon Nanotube Textile Sheets

UTD AUTHOR(S): Brian L. Brown, Julia S. Bykova, Austin R. Howard, Anvar A. Zakhidov and Mark Lee

Brown, Brian L., Julia S. Bykova, Austin R. Howard, Anvar A. Zakhidov, et al. 2014. "Microwave conductance of aligned multiwall carbon nanotube textile sheets." Applied Physics Letters 105(26): doi:10.1063/1.4905220.